

Parallel Magnetic Resonance Imaging

Martin Uecker

July 20, 2015

1 Introduction

The main disadvantages of Magnetic Resonance Imaging (MRI) are its long scan times and, in consequence, its sensitivity to motion. Exploiting the complementary information from multiple receive coils, parallel imaging is able to recover images from under-sampled k-space data and to accelerate the measurement [1, 2, 3, 4, 5, 6, 7]. Because parallel magnetic resonance imaging can be used to accelerate basically any imaging sequence it has many important applications. Parallel imaging brought a fundamental shift in image reconstruction: Image reconstruction changed from a simple direct Fourier transform to the solution of an ill-conditioned inverse problem. This work gives an overview of image reconstruction from the perspective of inverse problems. After introducing basic concepts such as regularization, discretization, and iterative reconstruction, advanced topics are discussed including algorithms for auto-calibration, the connection to approximation theory, and the combination with compressed sensing.

2 Parallel Imaging as Inverse Problem

2.1 Forward Model

The signal from a receive-coil array with N channels is given by [8]:

$$y_j(t) = \int_{\Omega} d\vec{r} m(\vec{r}) c_j(\vec{r}) e^{-2\pi i \vec{k}(t) \cdot \vec{r}} \quad 1 \leq j \leq N \quad (1)$$

The complex-valued magnetization image m represents the state of the transverse magnetization of the excited spins in the field-of-view (FOV) $\Omega \subset \mathbb{R}^d$ at the time of image acquisition. In MRI, typically a volume ($d = 3$) or a thin slice ($d = 2$) of proton spins is excited using a resonant radio-frequency pulse. The image (or volume) is modulated by the complex-valued sensitivities c_j of all receive coils (Fig. 1). The k-space signals $y_j(t)$ are then given by the Fourier transform of the coil images $c_j m$ sampled at discrete time points t_l along a given k-space trajectory $\vec{k}(t)$. Equation 1 neglects relaxation and off-resonance effects during the acquisition, which is possible if all samples at time points t_l

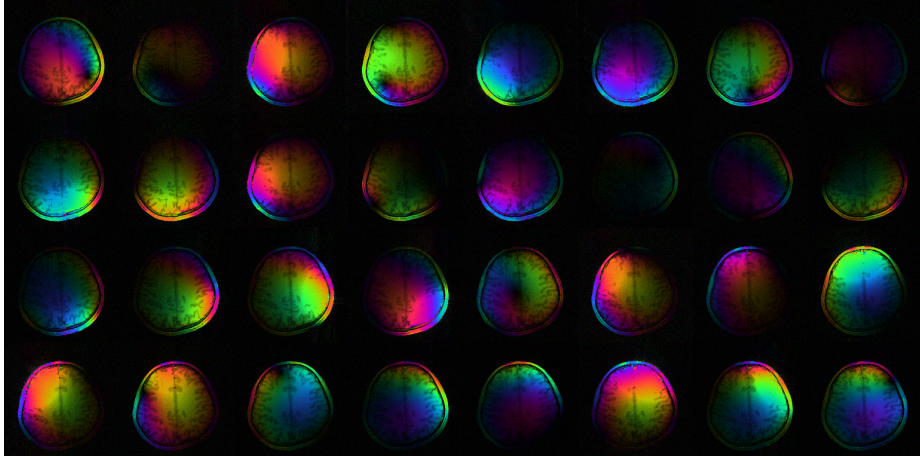


Figure 1: All individual coil images mc_j for a phased-array coil with 32 elements (channels). For each coil element $j = 1, \dots, 32$, the complex-valued magnetization image m is modulated by its unique receive sensitivity c_j . The phase is color coded.

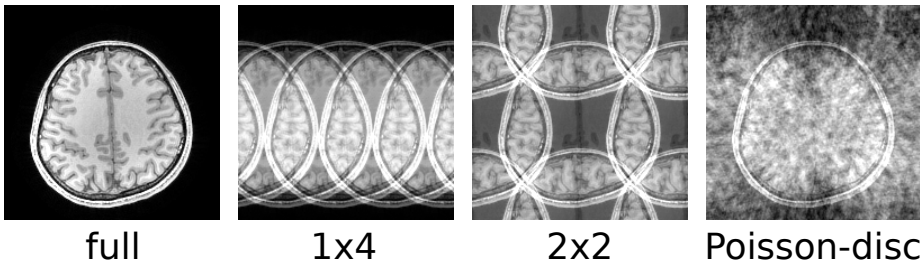


Figure 2: Under-sampling in k-space causes aliasing artifacts in the image domain. Images of a human brain were reconstructed with a direct Fourier transform from fully-sampled data (full) and four-fold under-sampled data (regular under-sampling in one dimension (1x4), two dimensions (2x2), and Poisson-disc sampling).

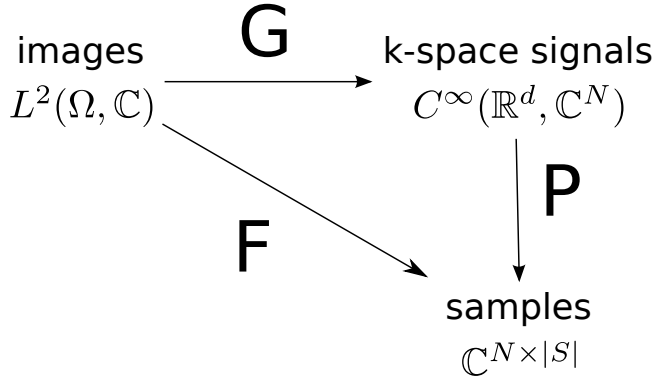


Figure 3: Parallel imaging is an inverse problem. The forward model is given by a composition of a physical model and a sampling operator $F = P \circ G$. The operator G maps magnetization images $m \in L(\Omega, \mathbb{C})$ on a field-of-view (FOV) Ω to the ideal k-space signals $f \in L(\mathbb{C}^d, \mathbb{C}^N)$ from N channels. The sampling operator P maps ideal signals f to k-space samples $f_j(\vec{k}(t_l))$ for all channels $j = 1, \dots, N$ and at all sample locations $\vec{k}(t_l) \in S$.

are acquired in a small window around the echo time (TE) after excitation. Relaxation and off-resonance effects from the excitation of the spins until the echo time are incorporated into the image and define the image contrast. Because in most cases it is not possible to acquire all data in this short acquisition window, samples have to be acquired in a repeated series of identical experiments, which always restore the magnetization image to exactly the same state.¹ This requirement to repeat the basic experiment many times is the reason for the long scan times in MRI. The goal of parallel imaging is to reduce the amount of data required to reconstruct images by optimally exploiting the complementary information from multiple receive coils. Although there are fundamental limits to the encoding power of the receive sensitivities, it has the potential to accelerate MRI by a factor of about four in each spatial dimension [9].

2.2 Image Reconstruction

If the coil sensitivities are known (e.g. from a pre-scan), image reconstruction for parallel imaging can be formulated as a linear inverse problem with discrete data [10]. Mathematically, the forward problem is given by an operator F which maps the magnetization image $m \in L(\Omega, \mathbb{C})$ of excited spins in a FOV $\Omega \subset \mathbb{R}^d$ to the sample values $y_j(t_l)$. This operator can be thought of as the composition

¹Single-shot Echo-Planar Imaging (EPI) and spiral imaging sequences acquire all data in a single acquisition. These sequences are fast, but image quality is compromised by blurring, distortions, and phase cancellation, due to relaxation and off-resonance effects. Parallel imaging can be used to shorten the acquisition window and reduce these artifacts.

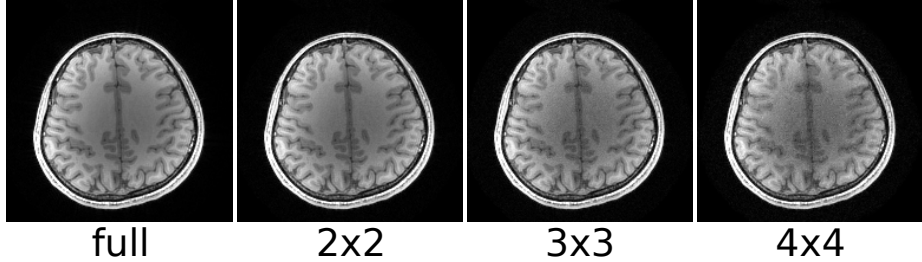


Figure 4: Images of a human brain reconstructed using parallel imaging from fully-sampled data (full) and under-sampled data (acceleration by 2x2, 3x3, and 4x4) acquired with a 32-channel coil. l_1 -wavelet regularization was used to suppress noise in the reconstruction.

$F = P \circ G$ of a physical model G for hypothetical multi-dimensional continuous k-space signals and a sampling operator P (see Fig. 3). The operator G is given by

$$G : L(\Omega, \mathbb{C}) \rightarrow C^\infty(\mathbb{R}^N, \mathbb{C}) \\ m \mapsto f \quad \text{with} \quad f_j(\vec{k}) = \langle m, enc^{j, \vec{k}} \rangle, \quad (2)$$

with the encoding functions defined as $enc^{j, \vec{k}}(\vec{r}) := \overline{c_j(\vec{r})} e^{+2\pi i \vec{k}(t) \cdot \vec{r}}$ and a scalar product defined on $L(\Omega, \mathbb{C})$ (anti-linear in the second argument). The sampling operator P evaluates the ideal k-space signals f_j at the sample locations $\vec{k}(t_l) \in S$ in k-space. It is assumed that the sampling process corresponds to the point-evaluation of ideal k-space functions, i.e. $y_j(t_l) = f_j(\vec{k}(t_l))$. The sample values $f_j(S)$ are corrupted by additive white Gaussian noise. Although the noise is typically correlated between receive channels, this correlation can be removed with a whitening step.

A variational solution to the inverse problem can be defined as the minimizer of a functional, i.e.

$$\hat{m}_\alpha := \operatorname{argmin}_x \|Fx - y\|_2^2 + \alpha R(x). \quad (3)$$

The functional is composed of a least-squares data fidelity term (which alternatively may also include weighting or use a robust norm [11, 12]) and an additional regularization term R . Discretized versions of this minimization problem are the basis of SMASH and SENSE parallel imaging methods [5, 6, 7, 13, 14]. For parallel MRI, this formulation has two advantages: First, arbitrary Cartesian or non-Cartesian sampling schemes can be used [14]. Second, the regularization term can be used to introduce prior knowledge about the solution.² Figure 4

²A third advantage - which conceptually goes beyond parallel imaging - is the possibility to extend the forward model to include further physical effects in model-based reconstruction, e.g. field maps [15, 16], motion-induced phase maps [17, 18], motion [19, 20], relaxation maps [21, 22, 23], or diffusion models [24], etc.

shows images of a human brain recovered from under-sampled data by numerical optimization of Equation 3.

2.3 Regularization

Ill-conditioning causes noise amplification during image reconstruction, which initially limited the application of parallel imaging to only moderate acceleration. This limitation can be overcome by incorporating prior knowledge about the image using regularization methods [25, 13, 26]. In the simplest case, regularization may consist of a basic quadratic penalty in the framework of a linear reconstruction, or make use of much more sophisticated techniques which exploit the structure of images but demand a non-linear reconstruction. For a least-squares problem with quadratic regularization, i.e. $R(x) = \|\sqrt{W}(x - x_0)\|_2^2$ with a positive definite operator W , the solution of Eq. 3 is explicitly given by the formula

$$\hat{m}_\alpha = x_0 + \underbrace{(F^H F + \alpha W)^{-1} F^H}_{F_\alpha^\dagger} (y - Fx_0) . \quad (4)$$

In the limit $\alpha \rightarrow 0$ this solution is called the best approximate and is given by the Moore-Penrose pseudo-inverse F^\dagger . It has a statistical interpretation - assuming white Gaussian noise - as the best unbiased estimate for the image. Regularization can be interpreted as prior knowledge and the optimizer as a maximum a posteriori (MAP) estimate of the image. Although regularization leads to a fundamental trade-off between bias and noise - which has to be chosen carefully for optimal image quality - it makes the use of higher acceleration possible. An optimal estimate in terms of mean squared error can only be obtained with regularization.

For optimal results, the prior knowledge should include as much specific knowledge about the image as possible. For example, regularization can exploit smoothness in the time domain [27], or exploit that changes relative to a fixed reference image x_0 can be assumed to be small. The later is used successfully for real-time MRI [28] or dynamic contrast enhanced (DCE) MRI [29]. While l_2 -regularization is simple to implement and already a clear improvement compared to unregularized parallel imaging, much better results can be obtained when using more advanced techniques such as l_1 -wavelet regularization, i.e. $R(x) = \|\text{DWT } x\|_1$, total variation, or other edge-preserving penalties [30, 31, 32, 33].

2.4 Discretization

Numerical reconstruction methods make use of discretization, i.e. the unknown image is expanded into a sum of basis functions:

$$m(\vec{r}) \approx \sum_l a_l g_l(\vec{r}) \quad (5)$$

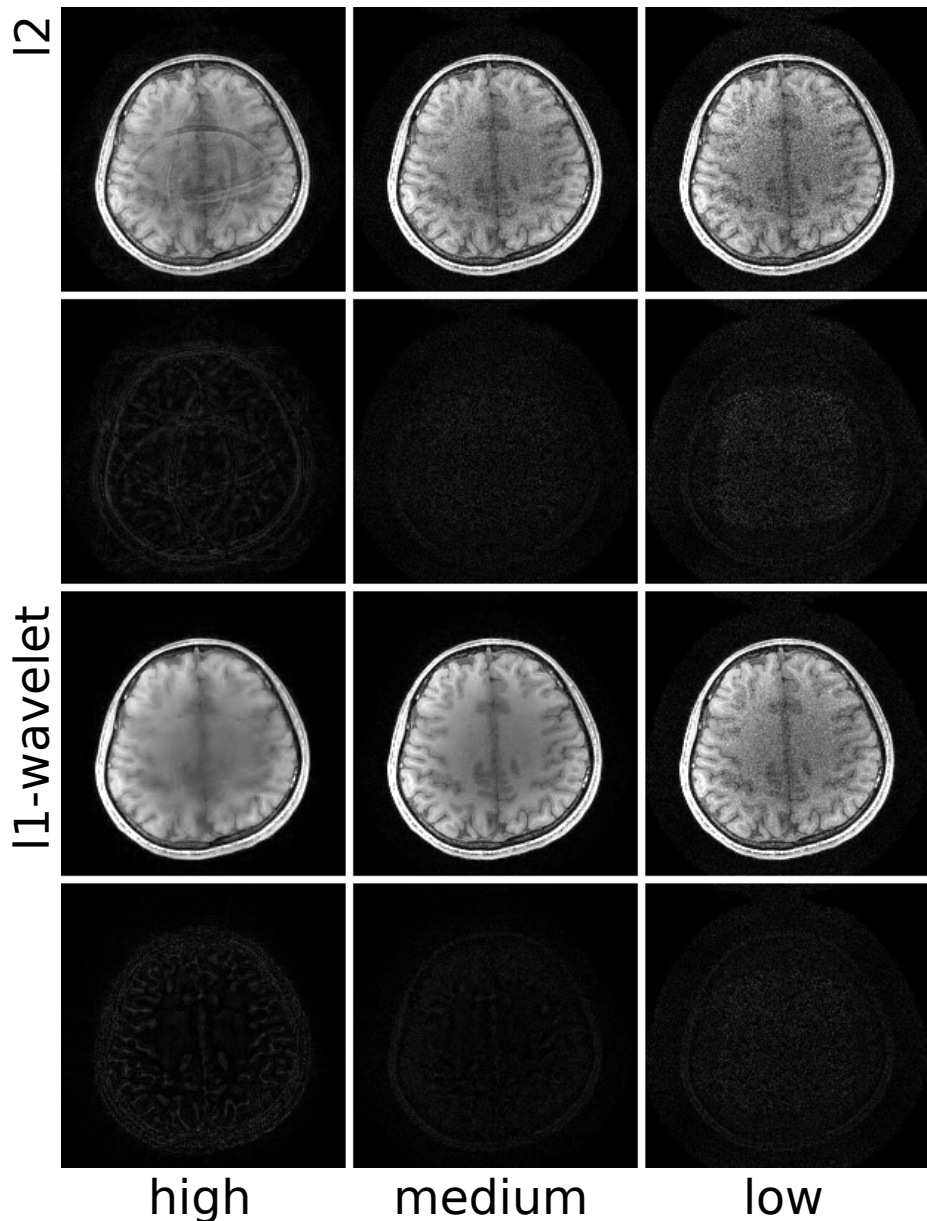


Figure 5: Reconstruction from 16-fold under-sampled data using low, medium, and high amount of l_2 and l_1 -wavelet regularization. Reconstructed images and difference images are shown. There is a trade-off between bias (residual artifacts, blurring) and noise depending on the amount of regularization.

Although the choice of this basis has subtle implications for results and interpretation, this topic has not drawn much attention.³ Most image-domain formulations based on SENSE use a grid of Dirac pulses to represent the image, because multiplication with the coil sensitivities in the forward model is then simply a point-wise multiplication. In contrast, k-space methods such as SMASH use a finite Fourier basis.

Discretization has a regularizing effect, i.e. the discretized problem might have better condition than the continuous problem. In parallel imaging, this effect can often be seen in the area outside of the sampled k-space region. Extrapolation to these areas causes high noise amplification [34]. A discretization scheme which excludes these degrees of freedom will be less affected by noise. On the other hand, a small basis leads to discretization errors because the solution can not be represented accurately. Both problems can be avoided by using fine discretization with a large number of basis functions and explicit regularization to control noise amplification [35].

It should be noted that for parallel imaging the ideal continuous solution of Eq. 3 can usually be computed almost perfectly [36]. Coil sensitivities are very smooth and can be approximated with a small number of Fourier coefficients (on an over-sampled FOV). The forward operator can then be understood as a convolution of the Fourier series of the image with a short filter. Because the acquired k-space data consists of a finite number of samples, also only a finite number of low-order Fourier coefficients from the infinite number of coefficients in the Fourier series of the image actually appear in the result of this convolution. For quadratic regularization, a minimum-norm solution is obtained when the infinite number of remaining higher-order coefficients are set to zero. An implementation of the forward operator requires an a-periodic convolution which can be implemented efficiently using a fast Fourier transform (FFT) algorithm. In practice this differs from a conventional SENSE implementation only by using zero padding and in the exact interpretation of the recovered coefficients.

For non-quadratic regularization, discretization errors may also arise in the implementation of the regularization terms. In general, oversampling can be used to reduce these errors. The combination of non-quadratic regularization and oversampling can also avoid artifacts caused by truncation of the signal in the Fourier domain (Gibbs ringing) [37]. Finally, an important aspect related to discretization is a common error called an “inverse crime” [38]: When testing a reconstruction algorithms with simulated data, computing this data using the same discretization scheme as used for the reconstruction can result in highly misleading results. One possibility to avoid this error is the use of analytic phantoms [39].

2.5 Numerical Optimization

For regular sampling schemes and quadratic regularization, a solution can be computed directly with matrix inversion, because the equations decouple into

³Discussions in terms of “ideal voxel functions” (or “target voxel shapes”) can be found in earlier works [7, 13].

small systems [7]. Although very efficient, this approach is not very flexible. Matrix-free iterative methods can be used instead to efficiently compute the solution for arbitrary sampling schemes [14]. Matrix-free methods are build from procedural implementations of the matrix-vector products $y \mapsto F^H y$ and $x \mapsto Fx$ (or $x \mapsto F^H Fx$). For Cartesian sampling, these operations can be implemented using point-wise multiplications and FFT algorithms. For non-Cartesian sampling, efficient non-uniform fast Fourier transform (nuFFT) algorithms have been developed to estimate samples at arbitrary k-space locations [40, 41, 42]. Even more efficient algorithms can be designed when considering the combined operator $F^H F$ which appears in the gradient of the least-squares data fidelity. For example, the effect of sampling in the Fourier domain can be computed exactly as a convolution with a truncated point-spread function with the use of two zero-padded FFTs [43]. Overlap-add and overlap-save convolution algorithms can be used to exploit the compact representation of the coil sensitivities in the Fourier domain [44].

For quadratic regularization, an efficient iterative algorithm is the conjugate gradient method applied to the normal equations [14]:

$$(F^H F + \alpha W) x = F^H y . \quad (6)$$

It should be noted that the use of a density compensation as known from the direct gridding algorithm is neither required nor recommended.⁴

For l_1 -regularization, the simplest (and slowest) reconstruction algorithm is iterative soft-thresholding [45]:

$$z_n = x_n + \alpha F^H (y - Fx_n) \quad (7)$$

$$x_n = T^{-1} \eta_\lambda(Tz_n) \quad (8)$$

The first equation is a gradient descent step and the second update uses soft-thresholding η in a transform basis T , e.g. a discrete wavelet transform. This scheme converges slowly, but can be accelerated with the addition of a ravine step as in FISTA [46, 47]. Especially when using multiple convex penalties R_n , a very flexible approach is an extension of the Alternating Direction Method of Multipliers (ADMM) [48, 49, 50] that can solve optimization problems of the form

$$\operatorname{argmin}_x \sum_{n=1}^L R_n(B_n x) . \quad (9)$$

This approach is very flexible and has many advantages from an implementation point of view, because it splits the optimization into independent sub-problems.

⁴In (non-iterative) gridding, the density compensation is a diagonal matrix which approximates the inverse of $F^H F$. Combined with the adjoint F^H it yields an approximation of the pseudo-inverse, i.e. $F^H D \approx F^\dagger$. Including a density compensation into an iterative optimization method produces solutions different from the optimal least-squares solution [14]. I.e., naively using $F^H D$ instead of F^H as is sometimes suggested to improve the condition yields a different optimization problem: $\operatorname{argmin}_x \|\sqrt{D}(Fx - y)\|_2^2 + \alpha R(x)$

Many different kinds of regularization terms can easily be integrated if respective proximal operators of the form

$$\text{prox}_\rho^R(y) := \operatorname{argmin}_x \frac{\rho}{2} \|x - y\|_2^2 + R(x) \quad (10)$$

are available in a computationally efficient form. For example, the proximal operator for the data fidelity term is the l_2 -regularized least-square inverse which can be computed efficiently with the methods of conjugate gradients. The proximal operator for l_1 -regularization can be evaluated simply using soft-thresholding. Efficient implementations of many advanced algorithms which make use of parallel programming can be found Berkeley Advanced Reconstruction Toolbox (BART) [51].

3 Auto-calibration

To obtain optimal results in parallel MRI, accurate and up-to-date information about the sensitivities of all receive coils is required. While approximate coil sensitivities can be computed from the geometry of the receive coils using the Bios Savart law, exact sensitivities depend on the loading of the coils and need to be determined with high accuracy during the actual measurement. A pre-scan can provide accurate calibration information, but this requires that experimental conditions stay exactly the same for the duration of the whole examination. Because this is not always guaranteed, auto-calibration methods have been developed which perform calibration using a small amount of additional data acquired during each individual scan [52, 53, 54, 55]. Because this reduces overall acceleration, optimal calibration from a minimum amount of data is desired. Two advanced techniques are described in the following: Joint estimation techniques simultaneously estimate image content and coil sensitivities from all data, which minimizes the amount of additional calibration data required. Subspace methods do not directly estimate sensitivities, but learn a signal subspace from calibration data. These algorithms can adapt to experimental conditions that violate the sensitivity-based signal model formulated in Equation 1. For this reason, they are more robust to certain kinds of errors.

3.1 Non-linear Inverse Reconstruction

Starting with the signal equation (Eq. 1), but now considering both image and coil sensitivities as unknowns, one obtains a non-linear inverse problem related to blind multi-channel deconvolution. Modelling the coil sensitivities as smooth functions in a Sobolev space $H^l(\Omega, \mathbb{C}^N)$, the non-linear version of the forward operator can be written as:

$$\begin{aligned} F : L_2(\Omega, \mathbb{C}) \times H^l(\Omega, \mathbb{C}^N) &\rightarrow C^\infty(\mathbb{R}^d, \mathbb{C}^N) \\ x := (m, c_1, \dots, c_N) &\mapsto y \end{aligned} \quad (11)$$

Many auto-calibrating parallel imaging methods reduce the reconstruction problem to a linear problem by first estimating the sensitivities c_j from a subset of the data and then solving for the image using these fixed estimates using a conventional linear reconstruction. Because this is sub-optimal, improved algorithms have been developed, which solve the non-linear inverse problem [56, 57, 58].

In non-linear inversion [58], a regularized solution is defined as the solution of the minimization problem

$$(\hat{m}, \hat{c}_1, \dots, \hat{c}_N) = \operatorname{argmin}_x \|Fx - y\|_2^2 + \alpha R(m) + \beta \sum_{j=1}^N Q(c_j). \quad (12)$$

Here, a smoothness penalty $Q(c_j)$ restricts the solution to smooth coil sensitivities. The Iterative Regularized Gauss-Newton Method (IRGNM) [59] is used to iteratively update an estimate of the solution based on a linearization of the original problem:

$$\begin{aligned} x_{n+1} - x_n &= \operatorname{argmin}_{\Delta x} \|DF_{x_n} \Delta x + Fx_n - y\|_2^2 \\ &\quad + \alpha_n R(\Delta m + m_n) + \beta \sum_{j=1}^N Q(\Delta c_j + c_j) \end{aligned} \quad (13)$$

Here, DF_{x_n} is the Frechét derivative of F at the current estimate x_n and the regularization parameters α_n, β_n are reduced in each iteration step. The smoothness penalty can be chosen as $Q(c_j) = \|(1 + s\Delta)^l c_j\|_2^2$ (with some constants s, l). This penalty can be transformed into a l_2 -norm by expressing the sensitivities using Fourier coefficients re-scaled with a positive definite diagonal matrix, which avoids bad conditioning of the of the reconstruction problem. For quadratic regularization of the image, i.e. $R(x) = \|x - x_0\|_2^2$, the algorithm then has the explicit update rule

$$x_{n+1} - x_n = (DF_{x_n}^H DF_{x_n} + \alpha_n I)^{-1} (DF_{x_n}^H (y - Fx_n) + \alpha_n (x_n - x_0)). \quad (14)$$

Non-linear reconstruction methods can be applied to non-Cartesian sampling [60, 61, 62] and extended to include non-linear penalties [32, 63].

One limitation of non-linear methods is that they may need an initial guess close to solution to converge to the correct global minimum. While it is usually sufficient to set the image to a constant value and the coil sensitivities to zero, in some cases a guess closer to the true solution is required. In this case, any direct estimation method can be used to estimate a set of approximate coil sensitivities, which can then be used to initialize the non-linear method.

3.2 Calibration Matrix

The calibration matrix is a fundamental tool which can be used to formulate many auto-calibration methods. Reconstruction kernels in GRAPPA [53] and SPIRiT [64] are null-space vectors of this matrix [65]. The calibration matrix

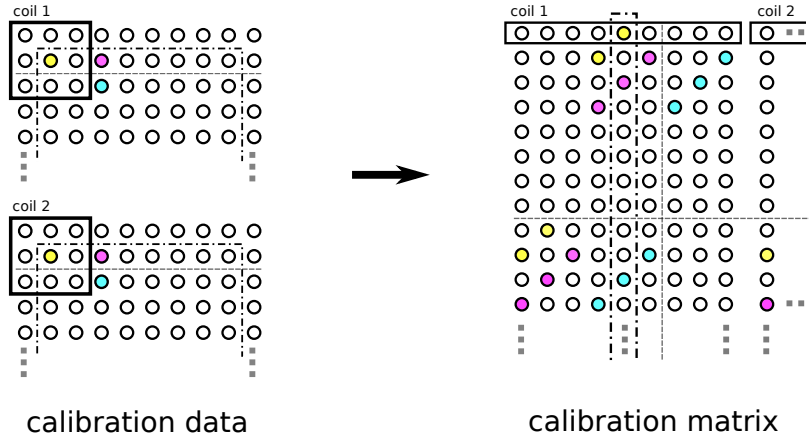


Figure 6: Construction of the calibration matrix: Overlapping blocks of the multi-channel k-space become rows of the calibration matrix.

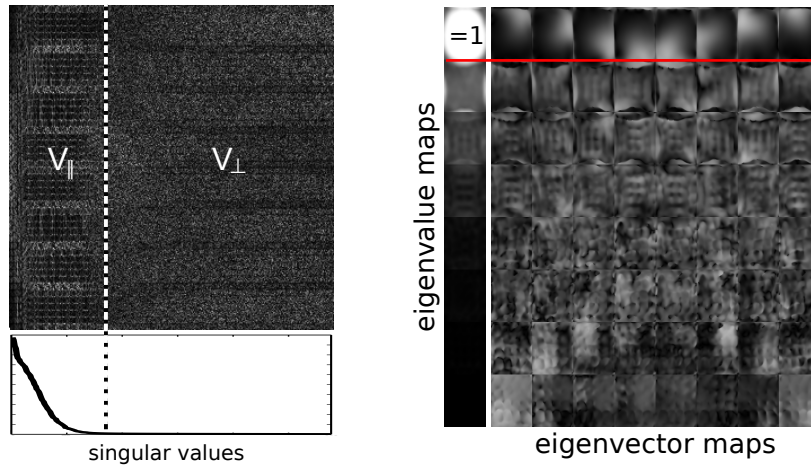


Figure 7: Left: Singular-Value-Decomposition (SVD) of the calibration matrix reveals signal V_{\parallel} and nullspace V_{\perp} . Right: A point-wise eigendecomposition of the operator $[\mathcal{F}^{-1} \mathcal{W} \mathcal{F}]$ is shown. This operator is derived from the nullspace condition $V_{\perp} R_k f = 0$ for each overlapping patch in k-space. The sensitivities (here: from an eight-channel coil) appear at each point as a eigenvector to eigenvalue one.

is a multi-dimensional multi-channel Casorati matrix constructed from fully-sampled patches in a calibration area in the center of k-space (see Fig. 6). It is related to the trajectory matrix from singular spectrum analysis (SSA) [66], and also to the lag cross-covariance matrix, which can be estimated as $\hat{\Sigma} = \frac{1}{M} C^H C$ (with M a normalization constant). Because coil sensitivities are very smooth, multi-channel signals have correlations in small local k-space patches. This implies that the calibration matrix (and the lag cross-covariance matrix) are low-rank, i.e. have a small signal space and large null space (Fig. 7). If the calibration matrix is constructed from an incomplete k-space with missing samples, structured low-rank matrix completion can be used to recover a completed matrix, which is the basis of a calibration-less parallel imaging technique known as SAKE [67].

3.3 ESPIRiT

Coil-by-coil reconstruction was originally proposed because combination of all channels in SMASH-based parallel imaging sometimes caused phase cancellation [68, 53]. In combination with auto-calibration coil-by-coil reconstruction has a very advantageous side effect: The reconstruction becomes robust against certain kinds of inconsistencies - in particular reconstruction in a tight FOV [69]. The fundamental reason is that the coil-by-coil reconstruction operator does not enforce the strict signal model of sensitivity-based reconstruction schemes formulated in Eq. 1, but represents a convex relaxation of this model.

ESPIRiT is a new reconstruction algorithm which exploits this. Because of shift-invariance the null-space condition should be true for all patches in an ideal multi-channel k-space f . Let $R_{\vec{k}}$ be an operator which extracts a patch around a given k-space position \vec{k} , a least-squares version of this condition is then given by

$$\sum_{\vec{k}} R_{\vec{k}}^H V_{\perp} V_{\perp}^H R_{\vec{k}} f = 0. \quad (15)$$

This can be further transformed to a convolution-type coil-by-coil operator \mathcal{W} , which reproduces ideal k-space signals:

$$\sum_{\vec{k}} R_{\vec{k}}^H \left(I - V_{\parallel} V_{\parallel}^H \right) R_{\vec{k}} f = 0 \quad (16)$$

$$\underbrace{M^{-1} \sum_{\vec{k}} R_{\vec{k}}^H V_{\parallel} V_{\parallel}^H R_{\vec{k}} f}_{\mathcal{W}} = f \quad (17)$$

$$\mathcal{W}f = f \quad (18)$$

Here, M is the size of a single patch. Transforming \mathcal{W} into the image domain yields an operator $[\mathcal{F}^{-1} \mathcal{W} \mathcal{F}]$ which operates point-wise. Because \mathcal{W} reproduces ideal k-space signals, the image-domain version reproduces the vector of coil images $c_j m$ at each point \vec{r} , i.e. $[\mathcal{F}^{-1} \mathcal{W} \mathcal{F}] c_j(\vec{r}) m(\vec{r}) = c_j(\vec{r}) m(\vec{r})$. In other words,

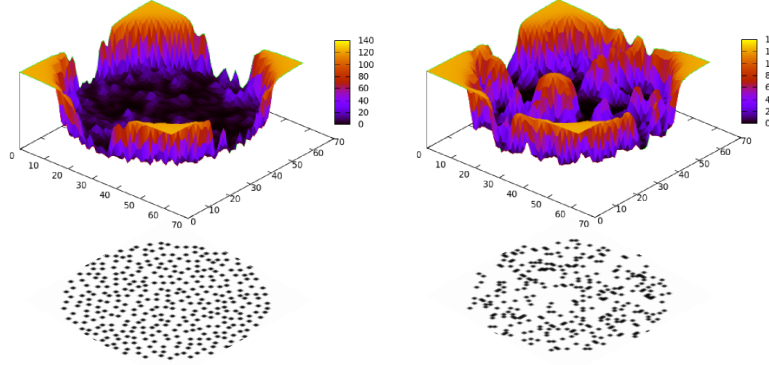


Figure 8: The power function for Poisson-disc and random sampling for a particular set of coil sensitivities. Outside of the sampled area and where random sampling leaves holes without samples the power function is high indicating that recovery of the k-space at this location has a high error when using parallel imaging.

everywhere where the image is non-zero the vector of sensitivities is a point-wise eigenvector to the eigenvalue 1 of the operator $[\mathcal{F}^{-1}\mathcal{W}\mathcal{F}]$. The eigenvector and eigenvalue maps from a point-wise eigendecomposition are shown in Figure 7. Together, these steps form a computational method to extract accurate coil sensitivities from the nullspace of the calibration matrix.

If the k-space is corrupted and does not fit the ideal model, multiple sets of sensitivities can appear in affected image regions as multiple eigenvectors to eigenvalue one. An extended forward model can take this additional information into account. Respective methods offer robustness to certain kinds of errors similar to auto-calibrating coil-by-coil methods such as GRAPPA [65].

4 Sampling and Reconstruction in k-Space

While the formulation of parallel imaging as an inverse problem is a powerful conceptual framework, additional theoretical tools are required to understand and evaluate different sampling schemes in k-space. For this purpose, a formulation of parallel imaging as approximation in a Reproducing Kernel Hilbert Space (RKHS) has recently been developed [34]. A RKHS is a Hilbert space of functions with continuous (bounded) point-evaluation functionals. This condition guarantees that sampling is compatible with the norm of the Hilbert space. This formulation of parallel imaging yields a unified framework to formulate and analyze sampling and reconstruction in k-space.

By identifying the norm of the signals in k-space with the norm of the corresponding images in $L(\Omega, \mathbb{C})$, it can be shown that the ideal k-space signals are

an RKHS with the matrix-valued kernel

$$K_{st}(\vec{k}, \vec{l}) = \int_{\Omega} d\vec{r} c_s(\vec{r}) \overline{c_t(\vec{r})} e^{-2\pi i \vec{r} \cdot (\vec{k} - \vec{l})}. \quad (19)$$

This kernel captures all local correlations in k-space induced by the sensitivities and exploited in parallel imaging algorithms for recovery of missing k-space samples. Given this kernel, a standard formula from approximation theory can be applied to obtain interpolation coefficients $u_j^{s, \vec{k}}$ for all channels $s = 1, \dots, N$ and known k-space samples $\vec{k} \in S$ for interpolation to arbitrary k-space positions:

$$\sum_{s=1}^N \sum_{\vec{k} \in S} K_{st}(\vec{k}, \vec{l}) u_j^{s, \vec{k}}(\cdot) = K_{jt}(\cdot, \vec{l}) \quad (20)$$

With these interpolation coefficients, unknown values in k-space can then be recovered from the acquired samples $f_j(\vec{k}(t_l))$ with the interpolation formula

$$\hat{f}_j(\vec{k}) = \sum_{t=1}^N \sum_{\vec{l} \in S} f_t(\vec{l}) u_j^{t, \vec{l}}(\vec{k}). \quad (21)$$

When no regularization is used in the computation of coefficients the recovered ideal k-space corresponds to the best approximate solution defined before. The interpolation formulas used in GRAPPA and SPIRiT and similar methods are local variants of this formula with an empirical estimate of the ideal kernel (Eq. 19). In addition to this interpolation formula, the link to approximation theory yields new insights into sampling in k-space. In particular, a point-wise error bound in k-space can be derived [70]:

$$|f_j(\vec{k}) - \hat{f}_j(\vec{k})|^2 \leq \|f\|^2 \cdot \underbrace{\left(K_{jj}(\vec{k}, \vec{k}) - \sum_{t=1}^N \sum_{\vec{l} \in S} K_{jt}(\vec{k}, \vec{l}) \overline{u_j^{t, \vec{l}}(\vec{k})} \right)}_{P_n^2(\vec{k})} \quad (22)$$

The power function P_j is computed from the kernel K and the interpolation functions u and depends only on the coil sensitivities and the sample locations. It can be used to analyze the properties of different sampling schemes for parallel imaging independent from any actual imaging data. Figure 8 shows the Power function for two different sampling schemes computed for a particular set of coil sensitivities.

5 Compressed Sensing Parallel Imaging

Compressed sensing is based on the idea that randomized under-sampling schemes produce incoherent noise-like artifacts in a transform domain which can then

be suppressed using denoising to iteratively recover the original signal [71, 72]. It exploits the compressibility of the image information, i.e. a sparse representation in a transform domain, to make the sparse signal coefficients stand out from the incoherent noise. Non-linear regularization terms can then be used to suppress the incoherent artifacts and recover a sparse representation of the image from the under-sampled data. Because MRI acquires data in the Fourier domain and is flexible enough to use almost arbitrary sampling schemes, this idea can be applied directly [31, 73].

Parallel imaging can be synergistic-ally combined with compressed sensing [31, 33, 64, 74]. This combination leads to exactly the same optimization problems already considered for parallel imaging alone, but requires incoherent sampling schemes suitable for compressed sensing. The most important schemes in practical use are variable-density Poisson-disc sampling and radial trajectories. Poisson-disc sampling guarantees that samples are not too close together. This would waste sampling time, because k-space positions which are close are highly correlated and can already be recovered using parallel imaging. Variable-density schemes have several advantages: They equalize the power spectrum of the missing samples, provide graceful degradation in case full recovery is not possible, and can be used for auto-calibrating parallel imaging when the k-space center is fully sampled. Methods which combine parallel imaging and compressed sensing represent the state of the art in image reconstruction, as demonstrated by their use in demanding applications such as in pediatric imaging without sedation [75, 76, 12]. Figure 9 shows an image from a pediatric patient reconstructed with parallel imaging compressed sensing at an acceleration factor of about seven.

6 Conclusion

Image reconstruction for parallel imaging can be formulated as an inverse problem. Based on this formulation, advanced iterative algorithms can be developed which (1) make use of optimal (Cartesian or non-Cartesian) sampling schemes, and (2) extend parallel imaging with advanced non-linear regularization terms. These ideas are combined in recent methods for compressed sensing parallel imaging, which currently represent the state of the art in image reconstruction.

References

- [1] M. Hutchinson and U. Raft. Fast MRI data acquisition using multiple detectors. *Magn Reson Med*, 6:87–91, 1988.
- [2] J. R. Kelton, R. L Magin, and S. M. Wright. An algorithm for rapid image acquisition using multiple receiver coils. In *Proc. SMRM, 8th Annual Meeting*, page 1172, Amsterdam, 1989.



Figure 9: Parallel imaging compressed sensing reconstruction of an abdomen from a pediatric patient using l_1 -ESPIRiT. The acquisition made us of variable-density Poisson-disc sampling with an acceleration factor of seven.

- [3] D. Kwiat, S. Einav, and G. Navon G. A decoupled coil detector array for fast image acquisition in magnetic resonance imaging. *Med Phys*, 18:251–265, 1991.
- [4] J. W. Carlson and T. Minemura. Imaging time reduction through multiple receiver coil data acquisition and image reconstruction. *Magn Reson Med*, 29:681–688, 1993.
- [5] J. B. Ra and C. Y. Rim. Fast imaging using subencoding data sets from multiple detectors. *Magn Reson Med*, 30:142–145, 1993.
- [6] D. K. Sodickson and W. J. Manning. Simultaneous acquisition of spatial harmonics (SMASH): Fast imaging with radiofrequency coil arrays. *Magn Reson Med*, 38:591–603, 1997.
- [7] K. P. Pruessmann, M. Weiger, M. B. Scheidegger, and P. Boesiger. SENSE: Sensitivity encoding for fast MRI. *Magn Reson Med*, 42:952–962, 1999.
- [8] P. B. Roemer, W. A. Edelstein, C. E. Hayes, S. P. Souza, and O. M. Mueller. The NMR phased array. *Magn Reson Med*, 16:192–225, 1990.
- [9] F. Wiesinger, P. Boesiger, and K. P. Pruessmann. Electrodynamics and ultimate SNR in parallel MR imaging. *Magn Reson Med*, 52:376–390, 2004.

- [10] M. Bertero, C. De Mol, and E. R. Pike. Linear inverse problems with discrete data. i. general formulation and singular system analysis. *Inverse Problems*, 1:301–330, 1985.
- [11] K. M. Johnson, W. F. Block S. B. Reeder, and A. Samsonov. Improved least squares mr image reconstruction using estimates of k-space data consistency. *Magn Reson Med*, 67:1600–1608, 2012.
- [12] J. Y. Cheng, T. Zhang, N. Ruangwattanapaisarn, M. T. Alley, M. Uecker, J. Pauly, M. Lustig, and S. S. Vasanawala. Free-breathing pediatric MRI with nonrigid motion correction and acceleration. *J Magn Reson Imaging*, 2014. DOI: 10.1002/jmri.24785.
- [13] D. K. Sodickson and C. A. McKenzie. A generalized approach to parallel magnetic resonance imaging. *Med Phys*, 28:1629–1643, 2001.
- [14] K. P. Pruessmann, M. Weiger, P. Börnert, and P. Boesiger. Advances in sensitivity encoding with arbitrary k-space trajectories. *Magn Reson Med*, 46:638–651, 2001.
- [15] B. P. Sutton, D. C. Noll, and J. A. Fessler. Fast, iterative image reconstruction for MRI in the presence of field inhomogeneities. *IEEE Trans Med Imaging*, 22:178–188, 2003.
- [16] B. P. Sutton, D. C. Noll, and J. A. Fessler. Dynamic field map estimation using a spiral-in/spiral-out acquisition. *Magn Reson Med*, 51:1194–1204, 2004.
- [17] C. Liu, M. E. Moseley, and R. Bammer. Simultaneous phase correction and SENSE reconstruction for navigated multi-shot DWI with non-cartesian k-space sampling. *Magn Reson Med*, 54:1412–1422, 2005.
- [18] M. Uecker, A. Karaus, and J. Frahm. Inverse reconstruction method for segmented multishot diffusion-weighted MRI with multiple coils. *Magn Reson Med*, 62:1342–1348, 2009.
- [19] F. Odille, P.-A. Vuissoz, P.-Y. Marie, and J. Felblinger. Generalized reconstruction by inversion of coupled systems (GRICS) applied to free-breathing MRI. *Magn Reson Med*, 60:146–157, 2008.
- [20] J. Y. Cheng, M. T. Alley, C. H. Cunningham, S. S. Vasanawala, J. M. Pauly, and M. Lustig. Nonrigid motion correction in 3D using autofocusing with localized linear translations. *Magn Reson Med*, 68:1785–1797, 2012.
- [21] V. T. Olafsson, D. C. Noll, and J. A. Fessler. Fast joint reconstruction of dynamic r and field maps in functional MRI. *IEEE Trans Med Imaging*, 27:1177–1188, 2008.

- [22] C. Graff, Z. Li, A. Bilgin, M. I. Altbach, A. F. Gmitro, and E. W. Clarkson. Iterative T2 estimation from highly undersampled radial fast spin-echo data. In *Proceedings of the 14th ISMRM Annual Meeting*, page 925, Seattle, 2006.
- [23] K. T. Block, M. Uecker, and J. Frahm. Model-based iterative reconstruction for radial fast spin-echo MRI. *IEEE Trans Med Imaging*, 28:1759–1769, 2009.
- [24] C. L. Welsh, E. V. R. DiBella, G. Adluru, and E. W. Hsu. Model-based reconstruction of undersampled diffusion tensor k-space data. *Magn Reson Med*, 70:429–440, 2013.
- [25] K. King and L. Angelos. SENSE image quality improvement using matrix regularization. In *Proceedings of the 9th Annual Meeting of ISMRM*, page 1771, Glasgow, 2001.
- [26] F.-H. Lin, K. K. Kwong, J. W. Belliveau, and L. L. Wald. Parallel imaging reconstruction using automatic regularization. *Magn Reson Med*, 51:559–567, 2004.
- [27] G. Adluru, S. P. Awate, T. Tasdizen, R. T. Wihtaker, and E. V. R. DiBella. Temporally constrained reconstruction of dynamic cardiac perfusion MRI. *Magn Reson Med*, 57:1027–1036, 2007.
- [28] M. Uecker, S. Zhang, D. Voit, K.-D. Merboldt, and J. Frahm. Real time MRI: Recent advances using radial FLASH. *Imaging in Medicine*, 4:461–476, 2012.
- [29] B. Xu, P. Spincemaille, G. Chen, M. Agrawal, T. D. Nguyen, M. R. Prince, and Y. Wang. Fast 3d contrast enhanced MRI of the liver using temporal resolution acceleration with constrained evolution reconstruction. *Magn Reson Med*, 69:370–381, 2013.
- [30] A. Raj, G. Singh, R. Zabih, B. Kressler, Y. Wang, N. Schuff, and M. Weiner. Bayesian parallel imaging with edge-preserving priors. *Magn Reson Med*, 57:8–21, 2007.
- [31] K. T. Block, M. Uecker, and J. Frahm. Undersampled radial MRI with multiple coils. Iterative image reconstruction using a total variation constraint. *Magn Reson Med*, 57:1086–1098, 2007.
- [32] M. Uecker, K. T. Block, and J. Frahm. Nonlinear inversion with l1-wavelet regularization - application to autocalibrated parallel imaging. In *Proceedings of the 16th Annual Meeting of the ISMRM*, page 1479, Toronto, 2008.
- [33] B. Liu, K. King, M. Steckner, J. Xie, J. Sheng, and L. Ying. Regularized sensitivity encoding (SENSE) reconstruction using Bregman iterations. *Magn Reson Med*, 61:145–152, 2009.

- [34] V. Athalye, M. Lustig, and M. Uecker. Parallel magnetic resonance imaging as approximation in a reproducing kernel Hilbert space. *Inverse Problems*, 31:045008, 2015.
- [35] J. Tsao, J. Sánchez, P. Boesiger, and K. P. Pruessmann. Minimum-norm reconstruction for optimal spatial response in high-resolution SENSE imaging. In *Proceedings of the 11th ISMRM Annual Meeting*, page 0014, Toronto, 2003.
- [36] M. Uecker. *Nonlinear Reconstruction Methods for Parallel Magnetic Resonance Imaging*. PhD thesis, Georg-August-Universität Göttingen, 2009.
- [37] K. T. Block, M. Uecker, and J. Frahm. Suppression of MRI truncation artifacts using total variation constrained data extrapolation. *International Journal of Biomedical Imaging*, 2008:184123, 2008.
- [38] D. Colton and R. Kress. *Inverse Acoustic and Electromagnetic Scattering Theory*. Springer, Berlin, 1992.
- [39] M. Guerquin-Kern, L. Lejeune, K. P. Pruessmann, and M. Unser. Realistic analytical phantoms for parallel magnetic resonance imaging. *IEEE Trans Med Imaging*, 31:626–636, 2012.
- [40] J. D. O’Sullivan. A fast sinc function gridding algorithm for Fourier inversion in computer tomography. *IEEE Trans Med Imaging*, 4:200–207, 1985.
- [41] J. I. Jackson, C.H. Meyer, D.G. Nishimura, and A. Macovski. Selection of a convolution function for Fourier inversion using gridding. *IEEE Trans Med Imaging*, 3:473–478, 1991.
- [42] P. J. Beatty, D. G. Nishimura, and J. M. Pauly. Rapid gridding reconstruction with a minimal oversampling ratio. *IEEE Trans Med Imaging*, 24:799–808, 2005.
- [43] F. Wajer and K. P. Pruessmann. Major speedup of reconstruction for sensitivity encoding with arbitrary trajectories. In *Proceedings of the 9th Annual Meeting of the ISMRM*, page 767, Glasgow, 2001.
- [44] M. Uecker and M. Lustig. Memory-saving iterative reconstruction on overlapping blocks of k-space. In *Proceedings of the 21th Annual Meeting of the ISMRM*, page 2645, Salt Lake City, 2013.
- [45] I. Daubechies, M. Defrise, and C. De Mol. An iterative thresholding algorithm for linear inverse problems with a sparsity constraint. *Comm Pure Appl Math*, 57:1413–1457, 2004.
- [46] Y. Nesterov. A method of solving a convex programming problem with convergence rate $\mathcal{O}(1/k^2)$. *Soviet Mathematics Doklady*, 27:372–376, 1983.

- [47] A. Beck and M. Teboulle. A fast iterative shrinkage-thresholding algorithm for linear inverse problems. *SIAM Journal on Imaging Sciences* 2.1, pages 183–202, 2009.
- [48] S. Boyd, N. Parikh, E. Chu, B. Peleato, and J. Eckstein. Distributed optimization and statistical learning via the alternating direction method of multipliers. *Foundations and Trends in Machine Learning*, 3:1–122, 2011.
- [49] M. V. Afonso, J. M. Bioucas-Dias, and M. A. Figueiredo. An augmented Lagrangian approach to the constrained optimization formulation of imaging inverse problems. *IEEE Trans Image Process*, 20:681–95, 2011.
- [50] S. Ramani and J. A. Fessler. Parallel MR reconstruction using augmented Lagrangian methods. *IEEE Trans Med Imaging*, 30:694–706, 2011.
- [51] BART Developers. Berkeley Advanced Reconstruction Toolbox (BART). <http://mikgroup.github.io/bart/>.
- [52] P. M. Jakob, M. A. Griswold, R. R. Edelman, and D. K. Sodickson. AUTOSMASH: A self-calibrating technique for SMASH imaging. *Magnetic Resonance Materials in Physics, Biology and Medicine*, 7:42–54, 1998.
- [53] M. A. Griswold, P. M. Jakob, R. M. Heidemann, M. Nittka, V. Jellus, J. Wang, B. Kiefer, and A. Haase. Generalized autocalibrating partially parallel acquisitions (GRAPPA). *Magn Reson Med*, 47:1202–1210, 2002.
- [54] C. A. McKenzie, E. N. Yeh, M. A. Ohliger, M. D. Price, and D. K. Sodickson. Self-calibrating parallel imaging with automatic coil sensitivity extraction. *Magn Reson Med*, 47:529–538, 2002.
- [55] M. A. Griswold, D. O. Walsh, R. M Heidemann, A. Haase, and P. M. Jakob. The use of an adaptive reconstruction for array coil sensitivity mapping and intensity normalization. In *Proceedings of the 10th ISMRM Annual Meeting*, page 2410, Honolulu, 2002.
- [56] F. Bauer and S. Kannengiesser. An alternative approach to the image reconstruction for parallel data acquisition in MRI. *Math Methods Appl Sci*, 30:1437–1451, 2007.
- [57] L. Ying and J. Sheng. Joint image reconstruction and sensitivity estimation in SENSE (JSENSE). *Magn Reson Med*, 57:1196–1202, 2007.
- [58] M. Uecker, T. Hohage, K. T. Block, and J. Frahm. Image reconstruction by regularized nonlinear inversion – joint estimation of coil sensitivities and image content. *Magn Reson Med*, 60:674–682, 2008.
- [59] AB. Bakushinsky. Iterative methods for nonlinear operator equations without regularity. new approach. In *Dokl. Russian Acad. Sci*, volume 330, pages 282–284, 1993.

- [60] F. Knoll, C. Clason, M. Uecker, and R. Stollberger. Improved reconstruction in non-cartesian parallel imaging by regularized nonlinear inversion. In *Proceedings of the 17th ISMRM Annual Meeting*, page 2721, Honolulu, 2009.
- [61] J. Sheng, E. Wiener, B. Liu, F. Boada, and L. Ying. Improved self-calibrated spiral parallel imaging using JSENSE. *Medical Engineering & Physics*, 31:510–514, 2009.
- [62] M. Uecker, S. Zhang, and J. Frahm. Nonlinear inverse reconstruction for realtime MRI of the human heart using undersampled radial FLASH. *Magn Reson Med*, 63:1456–1462, 2010.
- [63] F. Knoll, C. Clason, K. Bredies, M. Uecker, and R. Stollberger. Parallel imaging with nonlinear reconstruction using variational penalties. *Magn Reson Med*, 67:34–41, 2012.
- [64] M. Lustig and J. M. Pauly. SPIRiT: Iterative self-consistent parallel imaging reconstruction from arbitrary k-space. *Magn Reson Med*, 64:457–471, 2010.
- [65] M. Uecker, P. Lai, M. J. Murphy, P. Virtue, M. Elad, J. M. Pauly, S. S. Vasanawala, and M. Lustig. ESPiRiT – an eigenvalue approach to auto-calibrating parallel MRI: Where SENSE meets GRAPPA. *Magn Reson Med*, 71:990–1001, 2014.
- [66] N. Golyandina, A. Korobeynikov, A. Shlemov, and K. Usevich. Multivariate and 2D extensions of singular spectrum analysis with the rsssa package. *Journal of Statistical Software*, 2015. (in press), arXiv:1309.5050 [stat.ME].
- [67] P. J. Shin, P. E. Z. Larson, M. A. Ohliger, M. Elad, J. M. Pauly, D. B. Vigneron, and M. Lustig. Calibrationless parallel imaging reconstruction based on structured low-rank matrix completion. *Magn Reson Med*, 72:959–970, 2014.
- [68] C. A. McKenzie, M. A. Ohliger, E. N. Yeh, M. D. Price, and D. K. Sodickson. Coil-by-coil image reconstruction with SMASH. *Magn Reson Med*, 46:619–623, 2001.
- [69] M. A. Griswold, S. Kannengiesser, R. M. Heidemann, J. Wang, and P. M. Jakob. Field-of-view limitations in parallel imaging. *Magn Reson Med*, 52:1118–1126, 2004.
- [70] Z. Wu and R. Schaback. Local error estimates for radial basis function interpolation of scattered data. *PIMA J Numer Anal*, 13:13–27, 1993.
- [71] D. L. Donoho. Compressed sensing. *IEEE Trans Inform Theory*, 52:1289–1306, 2006.

- [72] E. J. Candès, J. Romberg, and T. Tao. Robust uncertainty principle: Exact signal reconstruction from highly incomplete frequency information. *IEEE Trans Inform Theory*, 52:489–509, 2006.
- [73] M. Lustig, D. L. Donoho, and J. M. Pauly. Sparse MRI: The application of compressed sensing for rapid MR imaging. *Magn Reson Med*, 58:1182–1195, 2007.
- [74] R. Otazo, K. Dim, L. Axel, and D. K. Sodickson. Combination of compressed sensing and parallel imaging for highly accelerated first-pass cardiac perfusion MRI. *Magn Reson Med*, 64:767–776, 2010.
- [75] S. S. Vasanawala, M. T. Alley, B. A. Hargreaves, R. A. Barth, J. M. Pauly, and M. Lustig. Improved pediatric MR imaging with compressed sensing. *Radiology*, 256:607–616, 2010.
- [76] T. Zhang, J. Y. Cheng, A. G. Potnick, R. A. Barth, M. T. Alley, M. Uecker, M. Lustig, J. M. Pauly, and S. S. Vasanawala. Fast pediatric 3D free breathing abdominal dynamic contrast enhanced MRI with a high spatiotemporal resolution. *J Magn Reson Imaging*, 41:460–473, 2015.